ACS APPLIED MATERIALS & INTERFACES

www.acsami.org

Research Article

Emergence of Insulating Ferrimagnetism and Perpendicular Magnetic Anisotropy in 3d−5d Perovskite Oxide Composite Films for Insulator Spintronics

Zeliang Ren,◆ Bin Lao,◆ Xuan Zheng, Lei Liao, Zengxing Lu, Sheng Li, Yongjie Yang, Bingshan Cao, Lijie Wen, Kenan Zhao, Lifen Wang, Xuedong Bai, Xianfeng Hao, Zhaoliang Liao,* Zhiming Wang,* and Run-Wei Li

Cite This: *ACS Appl. Mater. Interfaces* 2022, 14, 15407−15414

Read Online

ACCESS | Metrics & More | Article Recommendations | Supporting Information

ABSTRACT: Magnetic insulators with strong perpendicular magnetic anisotropy (PMA) play a key role in exploring pure spin current phenomena and developing ultralow-dissipation spintronic devices, rendering them highly desirable to develop new material platforms. Here, we report the epitaxial growth of $La_{2/3}Sr_{1/3}MnO_3$ (LSMO)-$SrIrO_3$ (SIO) composite oxide films (LSMIO) with different crystalline orientations fabricated by a sequential two-target ablation process by pulsed laser deposition. The LSMIO films exhibit high crystalline quality with a homogeneous mixture of LSMO and SIO at an atomic level. Ferrimagnetic and insulating transport characteristics are observed, with the temperature-dependent electric resistivity well fitted by the Mott variable-range-hopping model. Moreover, the LSMIO films show strong PMA. By further constructing all-perovskite-oxide heterostructures of the ferrimagnetic insulator LSMIO and a strong spin-orbital-coupled SIO layer, pronounced spin Hall magnetoresistance (SMR) and spin Hall-like anomalous Hall effect (SH-AHE) were observed. These results illustrate the potential application of the ferrimagnetic insulator LSMIO in developing all-oxide ultralow-dissipation spintronic devices.

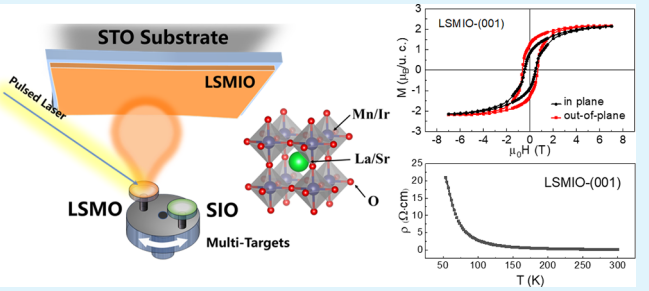

KEYWORDS: *perovskite oxide, magnetic insulator, perpendicular magnetic anisotropy, spin Hall magnetoresistance, spintronics*

INTRODUCTION

To satisfy the ever-increasing demand for information storage capacity and processing speed, reducing the energy consumption of electronic devices becomes increasingly important in the microelectronics industry. In contrast to conventional microelectronics relying only on the charge of electrons, spintronics uses the additional spin of electrons to encode, store, process, and transmit data, which is very promising to bring new capabilities to microelectronic devices.[1−3] Especially, spintronics based on ferromagnetic/ferrimagnetic magnetic insulators (FMIs) has attracted tremendous attention for developing ultralow-dissipation devices. The local magnetic moments in FMIs act as ideal media for pure spin angular momentum propagation, while the thermal consumptions such as Joule heating can be efficiently avoided by suppressing the movement of electrons.[4−6] Additionally, magnets with perpendicular magnetic anisotropy (PMA), where the magnetic easy axis preferentially points toward the normal to the surface, are essentially required to reduce the size of the device while maintaining high thermal stability.[7−11] A combination of FMIs and PMA further provides exciting functionalities for lowering the current threshold and enhancing the mobility of domain wall displacement, as well as achieving long decay length during spin-wave propagation.[12] Therefore, the development of FMIs with PMA is more meaningful for the development of high-performance spintronic devices.

Magnetic insulators are frequently found in transition-metal oxides with various crystal structures, such as rock salt, perovskite, spinel, and garnet. Among them, perovskite ABO_3 oxides are particularly promising candidates to achieve high-quality all-oxides spintronic devices because of their versatile functionalities, including spin source generator, spin current detector, and so on.[13,14] However, magnetic insulators in perovskites often favor antiferromagnetism instead of ferromagnetic ordering due to the superexchange interaction between neighboring magnetic ions according to Good-

Received: January 31, 2022
Accepted: March 14, 2022
Published: March 24, 2022

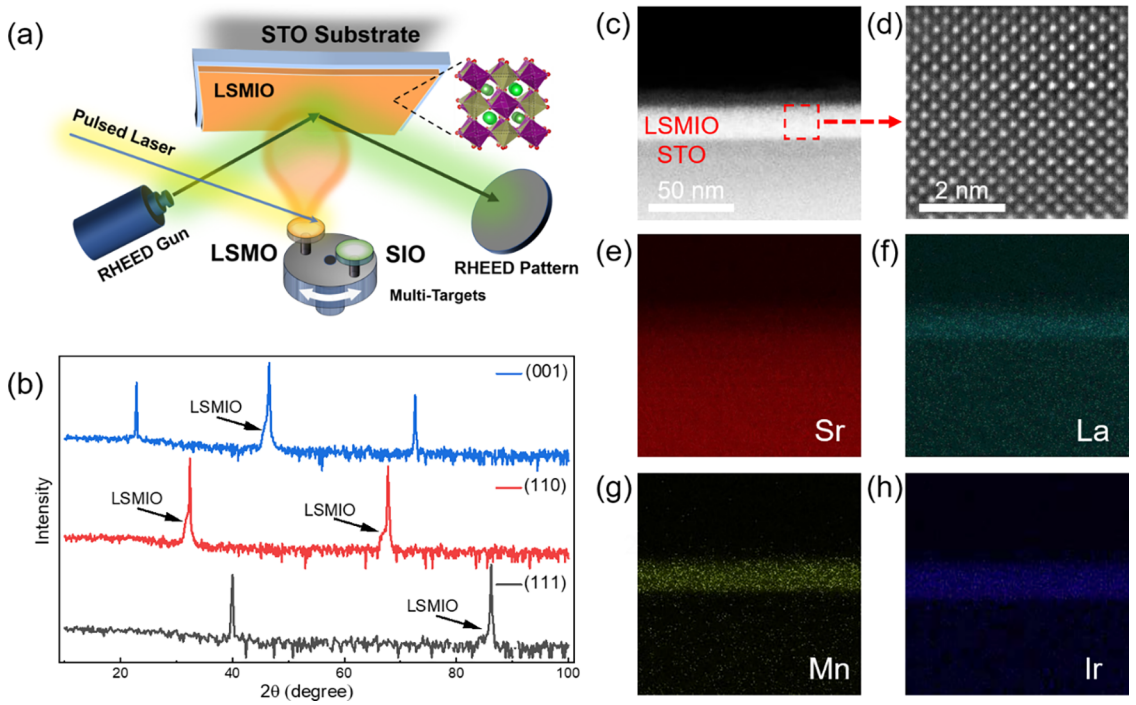

Figure 1. (a) Schematic illustration of the sequential two-target deposition process of LSMIO films. (b) XRD 2θ-θ scans of LSMIO films with the (001), (110), and (111) crystalline orientations. (c) HAADF-STEM images of the (001)-oriented LSMIO/STO. The high-magnification image in (b) corresponds to the single crystalline LSMIO films. (e–h) Corresponding EDS mappings of La, Mn, Ir, and Sr elements, respectively, confirming homogeneous cation distribution at the atomic level.

enough-Kanamori-Anderson rules.[15] Moreover, FMIs with strong PMA in perovskite oxides are rarely reported. Manganite $La_{1-x}Sr_xMnO_3$ (LSMO), as an archetypal colossal magnetoresistance material, has been widely studied on account of its rich phase diagrams, where multiple electric and magnetic properties are present.[16,17] Previous studies had demonstrated that PMA can be obtained in LSMO films and heterostructures by engineering the lattice and orbital degrees of freedom.[18−20] Recently, strong PMA could be triggered in LSMO when interfacing with strong spin-orbital-coupled $SrIrO_3$ (SIO).[21,22] However, the LSMO remained metallic in most cases, unless a large strain was imposed.[23−25] Through A- or/and B-site cation substitutions in ABO_3, the spin polarization of band structure can be directly controlled, leading to modified exchange interactions and associated magnetic and electrical ground states.[26] Thanks to the advances in epitaxial synthesis techniques, composite films have emerged as powerful platforms for realizing FMIs and strong PMA in LSMO-based perovskite oxides since deliberate control of specific atoms can be realized.[27] Given these reasons, emergent FMIs with strong PMA can be obtained via engineering cation substitution in LSMO and SIO, which enables exploring pure spin current phenomena in all-oxide heterostructures.

In this study, we report a facile method to fabricate LSMO-SIO (LSMIO) composite oxide films that are mixed homogenously at the atomic level. The LSMIO films are FMIs with PMA, whose temperature-dependent resistivity was fitted well by the Mott variable-range-hopping model. By further constructing heterostructures of FMI LSMIO and strong spin-orbital-coupled SIO layers, we explored pure spin current phenomena and observed pronounced spin Hall magnetoresistance (SMR) and spin Hall-like anomalous Hall effect (SH-AHE). These results demonstrate that FMI LSMIO is promising for exploring insulator spintronics in all-oxides heterostructures and developing low-dissipation spintronic devices.

RESULTS AND DISCUSSION

Figure 1a shows the schematics of the sequential two-target deposition process of LSMIO films by pulsed laser deposition (PLD). During the growth, the LSMO and SIO targets were rotated repeatedly and periodically. In each repeat, sub-monolayer 0.3 unit cell (u.c.) LSMO and 0.2 u.c. SIO were deposited, ensuring a homogeneous mixture of two ceramic targets at the atomic scale. The LSMIO films have a nominal stoichiometry of $La_{0.4}Sr_{0.6}Mn_{0.6}Ir_{0.4}O_3$. The crystalline orientation of LSMIO films can be controlled by changing the substrate orientation. The crystalline structures were characterized by X-ray diffraction (XRD) 2θ-θ scans, as shown in Figure 1b. The peaks of LSMIO films are labeled and are located on the left side of $SrTiO_3$ (STO) substrates closely. This result indicates that the films are slightly compressed (<0.1%) and of high-quality single-crystal without impurity phases. To further characterize the interface quality and structural homogeneity, scanning transmission electron microscopy (STEM) measurements on the (001)-oriented LSMIO films, as shown in Figure 1c–h, were performed. The sharp contrast across the LSMIO and STO substrates in Figure 1c, supplemented by a high-angle annular dark-field (HAADF) STEM image of the LSMIO films in Figure 1d, indicates the high crystalline quality of the films. Figure 1e–h shows the corresponding energy-dispersive X-ray spectroscopy (EDS) mappings of La, Sr, Mn, and Ir elements. All measured elements are distributed homogeneously at the atomic level in the composite films without observable clustering regions.

https://doi.org/10.1021/acsami.2c01849
ACS Appl. Mater. Interfaces 2022, 14, 15407−15414

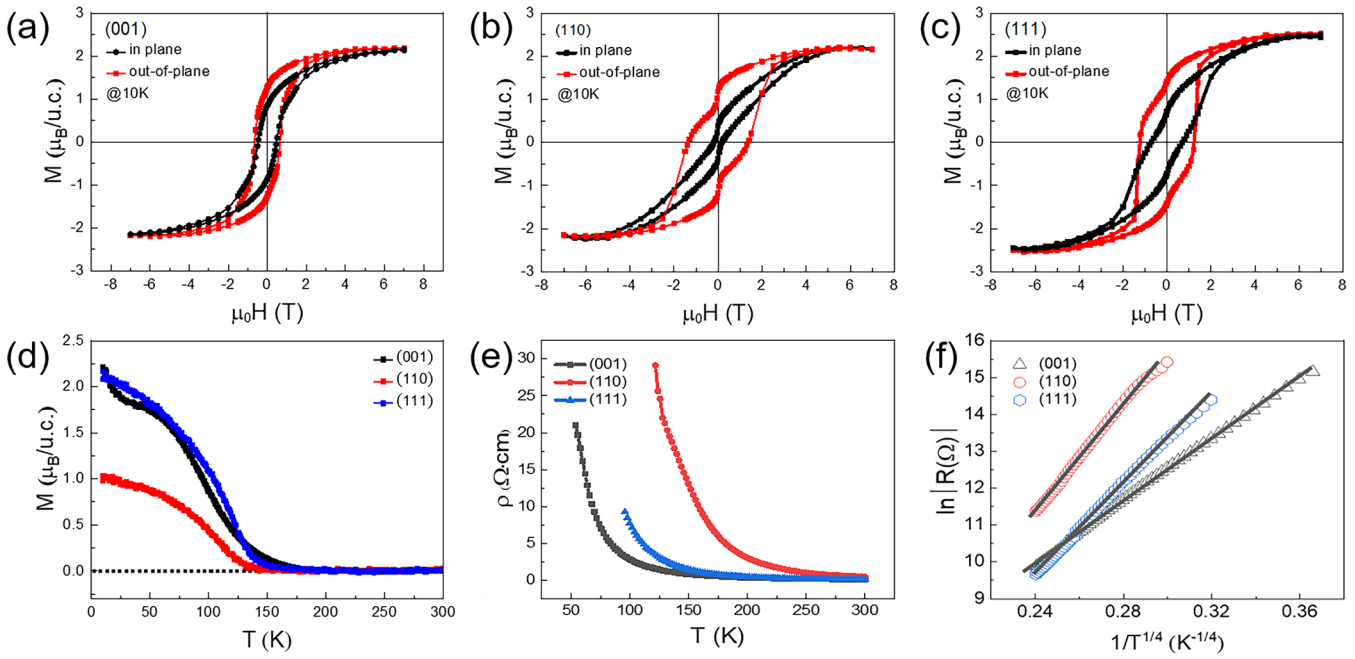

Figure 2. (a−c) Magnetic hysteresis loops measured with the magnetic field H applied along the in-plane (black) and out-of-plane (red) for LSMIO composite films with different crystalline orientations. (d−e) Corresponding magnetization M and electric resistivity as a function of temperature T for differently oriented LSMIO composite films. (f) Resistivity data are plotted with $\ln R \sim 1/T^{\wedge}[1/(d+1)]$ ($d = 3$) to fit with the three-dimensional Mott-VRH model.

To investigate the magnetic properties of LSMIO composite films, we measured magnetic hysteresis ($M-H$) loops and temperature-dependent magnetization ($M-T$) curves. Figure 2a−c shows the $M-H$ loops observed with the magnetic field applied perpendicular and parallel to the film plane for differently oriented LSMIO composite films. The coercive field was found to be 0.67 T, which was much larger than that of soft ferromagnetic LSMO films. On the other hand, we note that the saturation moment was determined to be around 2.4 μ_B/u.c., which was considerably smaller than that in LSMO films.[28] The reduction of the saturation moments can be explained by the antiferromagnetic coupling in the Mn−O−Ir bonds as evidenced from the first-principles calculations shown below, which leads to the ferrimagnetic ground state in LSMIO composite films. Figure 2d shows the corresponding magnetization M as a function of temperature. The Curie temperature (T_C) became lower for all of the LSMIO films as compared to pure LSMO bulk material. Intriguingly, by comparing the magnetic hysteresis loops measured under a field parallel and perpendicular to the film plane, it was found that all easy magnetization axes were perpendicular to the film plane for all LSMIO films regardless of the crystal orientation, while the magnetic anisotropy energies were 1.21×10^6, 1.55×10^6, and 1.56×10^6 erg/cm^3, respectively, which are comparable to the PMA reported in LSMO/SIO heterostructures.[22] Therefore, it is feasible to obtain perovskite FMIs with strong PMA in LSMIO composite films. Considering the negligible compressive strain imposed by the $SrTiO_3$ substrates, the observed strong PMA is not due to magnetoelastic anisotropy, as observed previously in LSMO films or heterostructures when under large compressive strain.[24,25] The strong PMA is due to the magnetic crystalline anisotropy originating from strong spin-orbital coupling and Mn−O−Ir bonding.[21,22,29]

To further understand the electrical properties of LSMIO composite films, we have performed the temperature-dependent electric resistivity measurements. As shown in Figure 2e, the resistivity increases monotonically as the temperature decreases, indicating that all of the LSMIO composite films are insulators. This is in sharp contrast to individual LSMO and SIO films, which are metallic and semimetallic in their bulk counterparts, respectively. To illustrate the origin of the emergent FMI state, we have fitted the resistivity data with thermal activation, Efros−Shklovskii variable-range-hopping (ES−VRH) and Mott variable-range-hopping (Mott-VRH) models, as shown in Figure S3b,c respectively. Figure 2f depicts the linear fitting curves using the Mott-VRH model, which agrees well with the measured resistivity. Here, the Mott-VRH model is expressed as the following equation

$$\rho(T) = \rho_{(0)}\exp(T_M/T)^{(1/d+1)} \quad (1)$$

where ρ_0 is the resistance coefficient, T_M is the characteristic temperature, and the exponent d depends on the VRH mechanism. For the Mott-VRH conduction, the exponent d is dimension-dependent and has a value of $d = 3$ in a three-dimensional system.[30−32] From the fitted characteristic temperature T_M, we can infer the Mott hopping energy (E_M) as

$$E_M = \frac{1}{4}k_B T(T_M/T)^{1/4} \quad (2)$$

The fitted hopping energies for (001)-, (110)-, and (111)-oriented LSMIO composite films were determined to be 72.2, 93.7, and 117.2 meV at room temperature (300 K), respectively. The Mott-VRH model describes that the localized electron at the Fermi level moves to another localized state in an optimum hopping distance, which is determined by the tradeoff between the lowest energy differences and the shortest hopping distances in a disordered system.[33] Given that the Mn−O−Ir bonds are dominant in the LSMIO composite oxide films, the Mott-VRH behavior suggests that the carriers hopping through the Mn−O−Ir bonds are suppressed and

https://doi.org/10.1021/acsami.2c01849
ACS Appl. Mater. Interfaces 2022, 14, 15407−15414

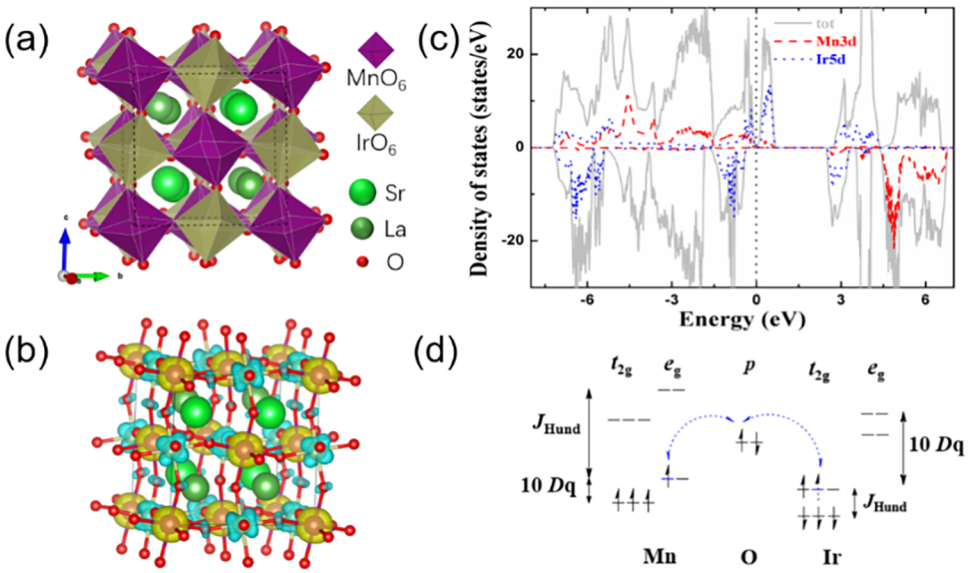

Figure 3. (a) Double perovskite structure of $LaSrMnIrO_6$, in which the Mn atoms (medium purple spheres) and the Ir atoms (medium brown ones) are surrounded by O_6 octahedron denoted by small red spheres, while the light (dark) green spheres are Sr (La) atoms. (b) Isosurfaces of the spin density (0.02 e/Å^2) for double perovskite $LaSrMnIrO_6$, within the ferrimagnetic magnetic ground state. Yellow and cyan colors denote spin up and spin down, respectively. (c) Total and partial density of states of Mn 3d and Ir 5d orbitals for $LaSrMnIrO_6$. Majority and minority spins are presented in the top and bottom channels, respectively. (d) Schematic representation of the superexchange interaction through the Mn−O−Ir bonds. The virtual electron hopping results in the antiferromagnetic coupling between Mn−O−Ir bonds.

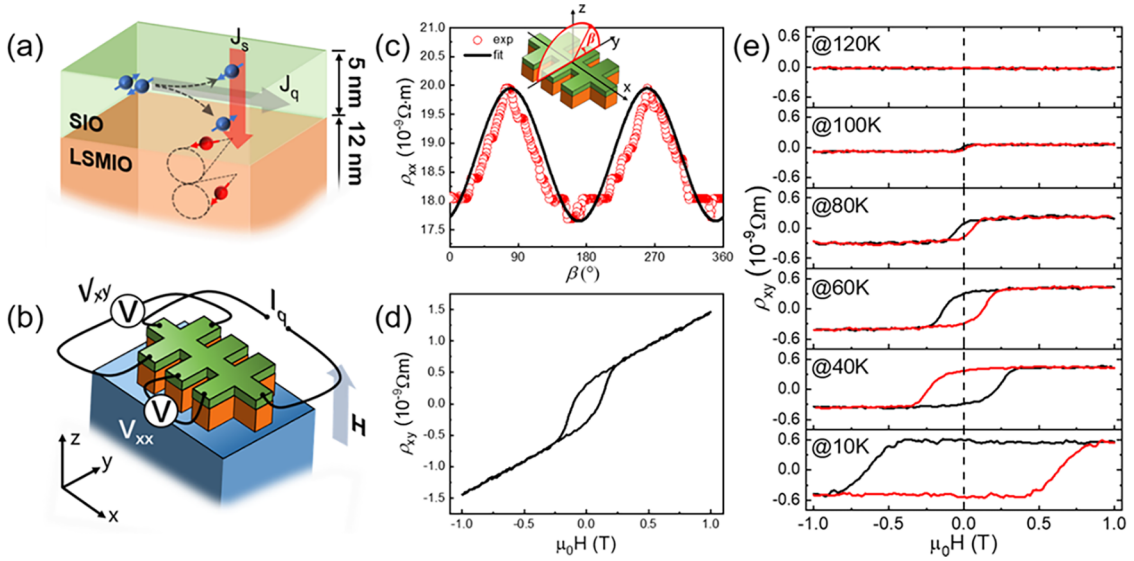

Figure 4. (a) Illustration of the SMR in the LSMIO/SIO heterostructure. (b) Schematic sample structure and measurement geometry. (c) Angle-dependent SMR signal. The inset shows the measurement geometry with an external field rotating in the $y-z$ plane around angle β. (d) Transverse Hall resistivity ρ_{xy} measured with the magnetic field applied perpendicular to the film plane. (e) Temperature-dependent AHE sign.

form localized states. This situation is in sharp contrast with metallic Mn−O−Mn bonds in LSMO films, where the electrons can itinerantly hop between neighboring Mn^{3+} and Mn^{4+} ions through the double-exchange mechanism.[17,34]

To gain further insight into the electronic and magnetic properties of LSMIO nanocomposite films, we have performed first-principles calculations based on the double perovskite model $LaSrMnIrO_6$ (Figure 3a). From the total energy results of the distinct magnetic solutions (schematically shown in Figure 4S and Table S2 in Supplementary Materials), we found that the ferrimagnetic, uncompensated antiferromagnetic alignment due to the unequal magnetic moments on Mn and Ir sites is the most stable state for LSMIO, confirming the experimental observations. Moreover, the GGA + U schemes prefer a quite stable magnetic solution with magnetic moments of Mn (~4.3 μ_B) and Ir (~−0.9 μ_B) ions, accompanied by considerable induced magnetic moments (~−0.1 μ_B) for all of the surrounding O^{2-} anions, as demonstrated in Figure 3b. Unexpectedly, the magnetic moment at Mn sites was slightly larger than the ideal spin-only 4 μ_B for Mn^{3+} cations, suggesting the special magnetic coupling mechanism behind it. Figure 3c shows that the ferrimagnetic ground state insulates with a band gap of 0.2 eV, which agrees well with the experimental temperature-dependent electric resistivity data. The antiferromagnetic coupling and unexpected large magnetic moment on the Mn^{3+} site can be interpreted in the framework

https://doi.org/10.1021/acsami.2c01849
ACS Appl. Mater. Interfaces 2022, 14, 15407−15414

of superexchange interactions through the virtual hopping bridged by O 2p spin-up electrons, as illustrated in Figure 3d, which is derived from the partial density of states and spin density plots. We can see that the virtual hopping from Ir $t_{2g}^{\uparrow}$ to the empty Mn $e_g^{\uparrow}$ via the bridged O $2p^{\uparrow}$ states accounts for the antiferromagnetic coupling and the abnormally large computed Mn^{3+} magnetic moment as well as the exclusively negative sign of the induced O^{2-} magnetic moments.

Finally, to explore the application of FMI LSMIO in a pure spin current phenomenon, we fabricated an LSMIO/SIO heterostructure and performed temperature-dependent magnetoresistance measurements. Figure 4a,b shows the schematic structure of Hall bar devices and measurement geometry. As illustrated in Figure 4a, the heterostructure consists of the FMI LSMIO and a strong spin-orbital coupled SIO layer. The SIO layer can efficiently convert the charge current into a spin current,[35,36] and so a pronounced SMR can be expected due to the asymmetry between absorption and reflection of the spin current at the LSMIO/SIO interface. Figure 4c shows the angle-dependent magnetoresistance measurements where the external field rotates in the $y-z$ plane around angle β. It is necessary to distinguish the difference between SMR and anisotropic magnetoresistance (AMR). The SMR signal is described as

$$\rho_{xx} = \rho_0 - \Delta\rho m_y^2 \tag{3}$$

while AMR signal is described as

$$\rho_{xx} = \rho_0 - \Delta\rho m_x^2 \tag{4}$$

In these two formulas, the ρ_0 is the constant resistivity offset, $\Delta\rho$ is the amplitude of the resistivity change as a function of the magnetization orientation, and m_i $(i = x, y)$ is the projection of the magnetization orientation unit vector along x- and y-axes in the coordinate system.[37−39] Note that $\rho_{xx} = \nu_{xx}wt/J_q l$ and $\rho_{xy} = \nu_{xy}t/J_q$, where w is the channel width (w = 10 um), l is the length of the separated voltage contacts (l = 50 um), and t is the thickness of the SIO layer (t = 5 nm). During the measurement, the external field was fixed to 4 T, which is much larger than the coercive field of LSMIO (0.67 T), to obtain collinear magnetization. Figure 4c shows that the resistivity data exhibit the $\cos^2\beta$ dependence. This is consistent with the SMR signal since m_y has $\cos\beta$ dependence, while AMR remains constant in angle β-dependent measurements since m_x is equal to 0. These measurements demonstrate that the SMR can be detected in all-perovskite-oxide heterostructures.

Figure 4d shows the Hall resistance measurements with the magnetic field applied perpendicular to the sample and varied from −4 to 4 T. By subtracting a linear contribution from the ordinary Hall effect, a clear hysteresis loop curve is visible, which resembles the AHE. Figure 4e shows the temperature-dependent Hall resistance after subtracting a linear term. The coercive field inferred from the Hall hysteresis loop is about 0.67 T at 10 K, which is similar to that of LSMIO films measured by SQUID shown in Figure 2a. Moreover, the coercive field decreases as a function of temperature and becomes invisible at above 120 K. These results demonstrate that the evolution of AHE with temperature resembles that of the magnetization versus temperature curve, as shown in Figure 2d, indicates that the observed AHE is closely related to the PMA of LSMIO composite films. We note that interfacial magnetism and AHE have been intensively studied in LSMO/SIO superlattices and heterostructures.[21,40−46] Our observed AHE is quite different from the AHE reported in ref 41, where a large AHE originates from SIO layers due to the magnetic proximity effect. Our AHE stems from the reflection of the spin current at the interface where an out-of-plane component (m_z) of the LSMIO magnetization rotates the spin orientation of the spin current and generates a transverse voltage via the inverse spin Hall effect (ISHE). Such AHE is termed SH-AHE.[47,48] Therefore, both SMR and SH-AHE indicate the occurrence of the spin transfer at the interface of the conductor and ferrimagnetic insulator. The spin current can be injected into insulators, which gives a possibility of transmitting spin information through an insulator. Such behavior would have an advantage of ultralow-power dissipation due to the absence of Joule heating.

CONCLUSIONS

In conclusion, we have synthesized LSMIO composite oxide films with different crystalline orientations by a sequential two-target deposition process. The LSMIO composite films exhibit high crystalline quality with a homogeneous mixture of LSMO and SIO at the atomic level. The electric and magnetic measurements, complemented by first-principles calculations, indicate that the LSMIO composite films are FMIs with strong PMA. The temperature-dependent electric resistivity is well described by the Mott-VRH model. Furthermore, by fabricating heterostructures of the FMI LSMIO and a strong spin-orbital-coupled SIO layer, we observed pronounced SMR and SH-AHE. These results illustrate the potential application of LSMIO in developing all-oxide ultralow-dissipation spintronic devices. Given the scarcity of perovskite FMIs with strong PMA, our result provides a promising real material candidate to boost the development of insulating spintronics devices.

EXPERIMENTAL SECTION

Sample Preparation. LSMIO composite films were synthesized by PLD, equipped with KrF (λ = 248 nm) excimer laser and high-reflection high-energy electron diffraction (RHEED). Prior to the film deposition, (001)-, (110)-, and (111)-oriented STO substrates were etched by NH_4F-buffered hydrofluoric acid, followed by annealing at 1100 °C for 90 min. During film deposition, the temperature of substrates, oxygen partial pressure, and laser fluence were set to 700 °C, 0.1 mbar, and 1.5 J/cm^2 at a frequency of 2 Hz, respectively. The film growth was monitored by RHEED, and the thickness was determined to be 12 nm.

Sample Characterizations. The quality and structure of the films were characterized by XRD (Bruker), STEM, and EDS (JEOL Grand ARM 300), respectively. The magnetic and electric properties were measured using the Quantum Design Magnetic Property Measurement System (MPMS−SQUID, Quantum Design) and Physical Property Measurement System (PPMS, Quantum Design). Further investigations of spin-related SMR and AHE were performed on Hall bar devices composed of LSMIO and SIO using a home-built low-temperature and high-intensity magnetic field magnetoelectric system. The LSMIO/SIO heterostructures were prepared by PLD under the same conditions as LSMIO films. The as-grown (001)-oriented LSMIO/SIO heterostructure was patterned into Hall bars by photolithography and Ar ion etching.

First-Principles Calculations. To describe the structure of LSMIO composite films, we constructed the canonical perovskite-type model within a 2 × 2 × 2 supercell ($La_4Sr_4Mn_4Ir_4O_{24}$, 40 atoms). The spin-polarized density functional theory (DFT) calculations were achieved with the plane-wave basis set as implemented in the Vienna *Ab initio* Simulation Package.[49,50] For the exchange−correlation

https://doi.org/10.1021/acsami.2c01849
ACS Appl. Mater. Interfaces 2022, 14, 15407−15414

functional, the generalized gradient approximation (GGA) was used according to the Perdew−Burke−Ernzerhof scheme,[51] and GGA + U approaches[52,53] were also performed for including the static electron correlation, with the Hubbard U = 4 eV (2 eV) and Hund J = 0.8 eV (0.4 eV) for Mn 3d (Ir 5d) states. A plane-wave energy cutoff of 400 eV was employed. The k-point meshes over the total Brillouin zone were sampled by 4 × 4 × 4 and 6 × 6 × 6 grids constructed according to the Monkhorst−Pack scheme[54,55] for structural relaxations and electronic calculations, respectively. We optimized the lattice vectors, volumes, and internal atomic forces with the relaxation terminated once the total energies and residual atomic forces converged to $<1 \times 10^{-5}$ eV and <|0.01| eV/Å, respectively.

■ ASSOCIATED CONTENT

Supporting Information

The Supporting Information is available free of charge at https://pubs.acs.org/doi/10.1021/acsami.2c01849.

Structural characterization of LSMO and LSMIO/SIO heterostructure; structural characterization of LSMIO composite films by STEM; the fittings of measured resistivity of LSMIO; and details of DFT calculations (PDF)

■ AUTHOR INFORMATION

Corresponding Authors

Zhaoliang Liao − *National Synchrotron Radiation Laboratory, University of Science and Technology of China, Hefei 230026 Anhui, China;* orcid.org/0000-0003-1701-9456; Email: zliao@ustc.edu.cn

Zhiming Wang − *CAS Key Laboratory of Magnetic Materials and Devices, Ningbo Institute of Materials Technology and Engineering, Chinese Academy of Sciences, Ningbo 315201, China; Zhejiang Province Key Laboratory of Magnetic Materials and Application Technology, Ningbo Institute of Materials Technology and Engineering, Chinese Academy of Sciences, Ningbo 315201, China; Center of Materials Science and Optoelectronics Engineering, University of Chinese Academy of Sciences, Beijing 100049, China;* orcid.org/0000-0002-4854-2170; Email: zhiming.wang@nimte.ac.cn

Authors

Zeliang Ren − *Nano Science and Technology Institute, University of Science and Technology of China, Hefei 230026 Anhui, China; CAS Key Laboratory of Magnetic Materials and Devices, Ningbo Institute of Materials Technology and Engineering, Chinese Academy of Sciences, Ningbo 315201, China; Zhejiang Province Key Laboratory of Magnetic Materials and Application Technology, Ningbo Institute of Materials Technology and Engineering, Chinese Academy of Sciences, Ningbo 315201, China*

Bin Lao − *CAS Key Laboratory of Magnetic Materials and Devices, Ningbo Institute of Materials Technology and Engineering, Chinese Academy of Sciences, Ningbo 315201, China; Zhejiang Province Key Laboratory of Magnetic Materials and Application Technology, Ningbo Institute of Materials Technology and Engineering, Chinese Academy of Sciences, Ningbo 315201, China*

Xuan Zheng − *CAS Key Laboratory of Magnetic Materials and Devices, Ningbo Institute of Materials Technology and Engineering, Chinese Academy of Sciences, Ningbo 315201, China; Zhejiang Province Key Laboratory of Magnetic Materials and Application Technology, Ningbo Institute of Materials Technology and Engineering, Chinese Academy of Sciences, Ningbo 315201, China; New Materials Institute, University of Nottingham Ningbo China, Ningbo 315100, China*

Lei Liao − *Beijing National Laboratory for Condensed Matter Physics, Institute of Physics, Chinese Academy of Sciences, Beijing 100190, China*

Zengxing Lu − *CAS Key Laboratory of Magnetic Materials and Devices, Ningbo Institute of Materials Technology and Engineering, Chinese Academy of Sciences, Ningbo 315201, China; Zhejiang Province Key Laboratory of Magnetic Materials and Application Technology, Ningbo Institute of Materials Technology and Engineering, Chinese Academy of Sciences, Ningbo 315201, China*

Sheng Li − *CAS Key Laboratory of Magnetic Materials and Devices, Ningbo Institute of Materials Technology and Engineering, Chinese Academy of Sciences, Ningbo 315201, China; Zhejiang Province Key Laboratory of Magnetic Materials and Application Technology, Ningbo Institute of Materials Technology and Engineering, Chinese Academy of Sciences, Ningbo 315201, China*

Yongjie Yang − *CAS Key Laboratory of Magnetic Materials and Devices, Ningbo Institute of Materials Technology and Engineering, Chinese Academy of Sciences, Ningbo 315201, China; Zhejiang Province Key Laboratory of Magnetic Materials and Application Technology, Ningbo Institute of Materials Technology and Engineering, Chinese Academy of Sciences, Ningbo 315201, China*

Bingshan Cao − *Nano Science and Technology Institute, University of Science and Technology of China, Hefei 230026 Anhui, China; CAS Key Laboratory of Magnetic Materials and Devices, Ningbo Institute of Materials Technology and Engineering, Chinese Academy of Sciences, Ningbo 315201, China; Zhejiang Province Key Laboratory of Magnetic Materials and Application Technology, Ningbo Institute of Materials Technology and Engineering, Chinese Academy of Sciences, Ningbo 315201, China*

Lijie Wen − *CAS Key Laboratory of Magnetic Materials and Devices, Ningbo Institute of Materials Technology and Engineering, Chinese Academy of Sciences, Ningbo 315201, China; Zhejiang Province Key Laboratory of Magnetic Materials and Application Technology, Ningbo Institute of Materials Technology and Engineering, Chinese Academy of Sciences, Ningbo 315201, China; Key Laboratory of Applied Chemistry, College of Environmental and Chemical Engineering, Yanshan University, Qinhuangdao 066004, China*

Kenan Zhao − *CAS Key Laboratory of Magnetic Materials and Devices, Ningbo Institute of Materials Technology and Engineering, Chinese Academy of Sciences, Ningbo 315201, China; Zhejiang Province Key Laboratory of Magnetic Materials and Application Technology, Ningbo Institute of Materials Technology and Engineering, Chinese Academy of Sciences, Ningbo 315201, China*

Lifen Wang − *Beijing National Laboratory for Condensed Matter Physics, Institute of Physics, Chinese Academy of Sciences, Beijing 100190, China;* orcid.org/0000-0002-8468-5048

Xuedong Bai − *Beijing National Laboratory for Condensed Matter Physics, Institute of Physics, Chinese Academy of Sciences, Beijing 100190, China;* orcid.org/0000-0002-1403-491X

Xianfeng Hao − *Key Laboratory of Applied Chemistry, College of Environmental and Chemical Engineering, Yanshan*

University, Qinhuangdao 066004, China; orcid.org/0000-0002-0688-0358

Run-Wei Li − *CAS Key Laboratory of Magnetic Materials and Devices, Ningbo Institute of Materials Technology and Engineering, Chinese Academy of Sciences, Ningbo 315201, China; Zhejiang Province Key Laboratory of Magnetic Materials and Application Technology, Ningbo Institute of Materials Technology and Engineering, Chinese Academy of Sciences, Ningbo 315201, China; Center of Materials Science and Optoelectronics Engineering, University of Chinese Academy of Sciences, Beijing 100049, China;* orcid.org/0000-0003-3879-9834

Complete contact information is available at: https://pubs.acs.org/10.1021/acsami.2c01849

Author Contributions

◆Z.R. and B.L. contributed equally to this work. Z.W. designed the experiments. Z.R. performed sample growth. Structure characterization and magnetic and transport measurements were performed by Z.R., B.L., X.Z., Z.L., S.L., B.C., L.W., and K.Z., L.L., L.W., and X.B. performed STEM measurements. Z.R. and B.L. performed data analysis. X.H. performed first-principles calculations and data analysis. Z.R., B.L., X.H., Z.L., and Z.W. wrote the manuscript. All authors participated in discussions and approved the submitted manuscript.

Notes

The authors declare no competing financial interest.

■ ACKNOWLEDGMENTS

This work was supported by the National Key Research and Development Program of China (Nos. 2017YFA0303600, 2019YFA0307800), the National Natural Science Foundation of China (Nos. 12174406, U1832102, 11874367, 51931011, 51902322), the Key Research Program of Frontier Sciences, Chinese Academy of Sciences (No. ZDBS-LY-SLH008), the Thousand Young Talents Program of China, K.C. Wong Education Foundation (GJTD-2020-11), the 3315 Program of Ningbo, the Natural Science Foundation of Zhejiang province of China (No. LR20A040001), the Beijing National Laboratory for Condensed Matter Physics.

■ REFERENCES

(1) Bader, S. D.; Parkin, S. S. P. Spintronics. *Annu. Rev. Condens. Matter Phys.* **2010**, *1*, 71.

(2) Shiraishi, M.; Ikoma, T. Molecular Spintronics. *Phys. E* **2011**, *43*, 1295.

(3) Hirohata, A.; Yamada, K.; Nakatani, Y.; Prejbeanu, I.-L.; Diény, B.; Pirro, P.; Hillebrands, B. Review on Spintronics: Principles and Device Applications. *J. Magn. Magn. Mater.* **2020**, *509*, No. 166711.

(4) Bauer, G. E.; Saitoh, E.; van Wees, B. J. Spin Caloritronics. *Nat. Mater.* **2012**, *11*, 391.

(5) Kajiwara, Y.; Harii, K.; Takahashi, S.; Ohe, J.; Uchida, K.; Mizuguchi, M.; Umezawa, H.; Kawai, H.; Ando, K.; Takanashi, K.; Maekawa, S.; Saitoh, E. Transmission of Electrical Signals by Spin-wave Interconversion in a Magnetic Insulator. *Nature* **2010**, *464*, 262.

(6) Gilleo, M. A. Ferromagnetic Insulators: Garnets. *Handbook of Ferromagnetic Materials*; Elsevier, 1980; *2*, pp 1−53.

(7) Dieny, B.; Chshiev, M. Perpendicular Magnetic Anisotropy at Transition Metal/oxide Interfaces and Applications. *Rev. Mod. Phys.* **2017**, *89*, No. 025008.

(8) Mangin, S.; Ravelosona, D.; Katine, J. A.; Carey, M. J.; Terris, B. D.; Fullerton, E. E. Current-induced Magnetization Reversal in Nanopillars with Perpendicular Anisotropy. *Nat. Mater.* **2006**, *5*, 210.

(9) Ikeda, S.; Miura, K.; Yamamoto, H.; Mizunuma, K.; Gan, H. D.; Endo, M.; Kanai, S.; Hayakawa, J.; Matsukura, F.; Ohno, H. A Perpendicular-anisotropy CoFeB-MgO Magnetic Tunnel Junction. *Nat. Mater.* **2010**, *9*, 721−724.

(10) Wang, M.; Cai, W.; Cao, K.; Zhou, J.; Wrona, J.; Peng, S.; Yang, H.; Wei, J.; Kang, W.; Zhang, Y.; Langer, J.; Ocker, B.; Fert, A.; Zhao, W. Current-induced Magnetization Switching in Atom-thick Tungsten Engineered Perpendicular Magnetic Tunnel Junctions with Large Tunnel Magnetoresistance. *Nat. Commun.* **2018**, *9*, No. 671.

(11) Wang, M.; Cai, W.; Zhu, D.; Wang, Z.; Kan, J.; Zhao, Z.; Cao, K.; Wang, Z.; Zhang, Y.; Zhang, T.; Park, C.; Wang, J.-P.; Fert, A.; Zhao, W. Field-free Switching of a Perpendicular Magnetic Tunnel Junction through the Interplay of Spin−orbit and Spin-transfer Torques. *Nat. Electron.* **2018**, *1*, 582.

(12) Vélez, S.; Schaab, J.; Wornle, M. S.; Muller, M.; Gradauskaite, E.; Welter, P.; Gutgsell, C.; Nistor, C.; Degen, C. L.; Trassin, M.; Fiebig, M.; Gambardella, P. High-speed Domain Wall Racetracks in a Magnetic Insulator. *Nat. Commun.* **2019**, *10*, No. 4750.

(13) Tokura, Y.; Kawasaki, M.; Nagaosa, N. Emergent Functions of Quantum Materials. *Nat. Phys.* **2017**, *13*, 1056.

(14) Bhattacharya, A.; May, S. J. Magnetic Oxide Heterostructures. *Annu. Rev. Mater. Sci.* **2014**, *44*, 65.

(15) Goodenough, J. B. *Magnetism and the Chemical Bond*; Interscience Publishers, a division of John Wiley & Sons: New York, London, 1963.

(16) Hemberger, J.; Krimmel, A.; Kurz, T.; Krug von Nidda, H. A.; Ivanov, V. Y.; Mukhin, A. A.; Balbashov, A. M.; Loidl, A. Structural, Magnetic, and Electrical Properties of Single-crystalline $La_{1-x}Sr_xMnO_3$($0.4<x<0.85$). *Phys. Rev. B* **2002**, *66*, No. 094410.

(17) Cesaria, M.; Caricato, A. P.; Maruccio, G.; Martino, M. LSMO − Growing Opportunities by PLD and Applications in Spintronics. *J. Phys.: Conf. Ser.* **2011**, *292*, No. 012003.

(18) Zhang, J.; Chen, X.; Zhang, Q.; Han, F.; Zhang, J.; Zhang, H.; Zhang, H.; Huang, H.; Qi, S.; Yan, X.; Gu, L.; Chen, Y.; Hu, F.; Yan, S.; Liu, B.; Shen, B.; Sun, J. Magnetic Anisotropy Controlled by Distinct Interfacial Lattice Distortions at the $La_{1-x}Sr_xCoO_3$/$La_{2/3}Sr_{1/3}MnO_3$ Interfaces. *ACS Appl. Mater. Interfaces* **2018**, *10*, 40951.

(19) Zhang, J.; Zhong, Z.; Guan, X.; Shen, X.; Zhang, J.; Han, F.; Zhang, H.; Zhang, H.; Yan, X.; Zhang, Q.; Gu, L.; Hu, F.; Yu, R.; Shen, B.; Sun, J. Symmetry Mismatch-driven Perpendicular Magnetic Anisotropy for Perovskite/brownmillerite Heterostructures. *Nat. Commun.* **2018**, *9*, No. 1923.

(20) Han, F.; Chen, X.; Wang, J.; Huang, X.; Zhang, J.; Song, J.; Liu, B.; Chen, Y.; Bai, X.; Hu, F.; et al. Perpendicular Magnetic Anisotropy Induced by $La_{2/3}Sr_{1/3}MnO_3$−$YBaCo_2O_{5+\delta}$ Interlayer Coupling. *J. Phys. D: Appl. Phys.* **2021**, *54*, No. 185302.

(21) Nichols, J.; Gao, X.; Lee, S.; Meyer, T. L.; Freeland, J. W.; Lauter, V.; Yi, D.; Liu, J.; Haskel, D.; Petrie, J. R.; Guo, E. J.; Herklotz, A.; Lee, D.; Ward, T. Z.; Eres, G.; Fitzsimmons, M. R.; Lee, H. N. Emerging Magnetism and Anomalous Hall Effect in Iridate-manganite Heterostructures. *Nat. Commun.* **2016**, *7*, No. 12721.

(22) Yi, D.; Flint, C. L.; Balakrishnan, P. P.; Mahalingam, K.; Urwin, B.; Vailionis, A.; N'Diaye, A. T.; Shafer, P.; Arenholz, E.; Choi, Y.; Stone, K. H.; Chu, J. H.; Howe, B. M.; Liu, J.; Fisher, I. R.; Suzuki, Y. Tuning Perpendicular Magnetic Anisotropy by Oxygen Octahedral Rotations in ($La_{1-x}Sr_xMnO_3$)/($SrIrO_3$) Superlattices. *Phys. Rev. Lett.* **2017**, *119*, No. 077201.

(23) Wang, B.; You, L.; Ren, P.; Yin, X.; Peng, Y.; Xia, B.; Wang, L.; Yu, X.; Poh, S. M.; Yang, P.; Yuan, G.; Chen, L.; Rusydi, A.; Wang, J. Oxygen-driven Anisotropic Transport in Ultra-thin Manganite Films. *Nat. Commun.* **2013**, *4*, No. 2778.

(24) Xiao, Z.; Zhang, F.; Farrukh, M. A.; Wang, R.; Zhou, G.; Quan, Z.; Xu, X. Perpendicular Magnetic Anisotropy in Compressive Strained $La_{0.67}Sr_{0.33}MnO_3$ Films. *J. Mater. Sci.* **2019**, *54*, 9017−9024.

(25) Wu, Y.; Suzuki, Y.; Rüdiger, U.; Yu, J.; Kent, A. D.; Nath, T. K.; Eom, C. B. Magnetotransport and Magnetic Domain Structure in Compressively Strained Colossal Magnetoresistance Films. *Appl. Phys. Lett.* **1999**, *75*, 2295.

(26) Sun, L.; Zhang, J.; Chen, Y. B.; Zhang, S.-T.; Hong, B.; Zhao, J.; Luo, Z.; Chen, Y.-F. The Significant and Temperature-insensitive Magnetoresistance Observed in Co-doped $(La_{0.7}Sr_{0.3})MnO_3$ Thin Films. *AIP Adv.* **2019**, *9*, No. 015327.
(27) Huon, A.; Yoon, S.; Fitzsimmons, M. R.; Charlton, T. R.; Ok, J. M.; Cruz, Cd.; Lee, H. N. Effects of Sn Substitution in $SrRuO_3$ Epitaxial Films. *Appl. Phys. Lett.* **2021**, *119*, No. 112404.
(28) Feng, Y.; Jin, K. J.; Gu, L.; He, X.; Ge, C.; Zhang, Q. H.; He, M.; Guo, Q. L.; Wan, Q.; He, M.; Lu, H. B.; Yang, G. Insulating Phase at Low Temperature in Ultrathin $La_{0.8}Sr_{0.2}MnO_3$ Films. *Sci. Rep.* **2016**, *6*, No. 22382.
(29) Lu, Z.; Liu, J.; Wen, L.; Feng, J.; Kong, S.; Zheng, X.; Li, S.; Jiang, P.; Zhong, Z.; Zhu, J.; Hao, X.; Wang, Z.; Li, R.-W. Lateral Modulation of Magnetic Anisotropy in Tricolor 3d−5d Oxide Superlattices. *ACS Appl. Electron. Mater.* **2021**, *3*, 4210.
(30) Liu, X.; Yang, Y.; Zhang, Q.; Yan, D.; Lu, J.; Chen, R.; Shi, Y.; Xiong, C.; Wang, F.; Gu, L.; Zhang, J. Mott Gap Engineering in $Sr_2IrO_4/SrTiO_3$ Superlattices. *Sci. China Mater.* **2020**, *63*, 1855.
(31) Mott, N. Review article: The Mobility Edge Since 1967. *J. Phys., C: Solid State Phys.* **1987**, *20*, 3075.
(32) Chaurasia, R.; Asokan, K.; Kumar, K.; Pramanik, A. K. Low-temperature Ferromagnetism in Perovskite $SrIrO_3$ Films. *Phys. Rev. B* **2021**, *103*, No. 064418.
(33) Xue, J.; Huang, S.; Wang, J.-Y.; Xu, H. Q. Mott Variable-range Hopping Transport in a MoS_2 Nanoflake. *RSC Adv.* **2019**, *9*, 17885−17890.
(34) Lu, Z.; Liu, J.; Feng, J.; Zheng, X.; Yang, L.-h.; Ge, C.; Jin, K.-j.; Wang, Z.; Li, R.-W. Synthesis of Single-crystal $La_{0.67}Sr_{0.33}MnO_3$ Freestanding Films with Different Crystal-orientation. *APL Mater.* **2020**, *8*, No. 051105.
(35) Nan, T.; Anderson, T. J.; Gibbons, J.; Hwang, K.; Campbell, N.; Zhou, H.; Dong, Y. Q.; Kim, G. Y.; Shao, D. F.; Paudel, T. R.; Reynolds, N.; Wang, X. J.; Sun, N. X.; Tsymbal, E. Y.; Choi, S. Y.; Rzchowski, M. S.; Kim, Y. B.; Ralph, D. C.; Eom, C. B. Anisotropic Spin-orbit Torque Generation in Epitaxial $SrIrO_3$ by Symmetry Design. *Proc. Natl. Acad. Sci. U.S.A.* **2019**, *116*, 16186−16191.
(36) Everhardt, A. S.; Dc, M.; Huang, X.; Sayed, S.; Gosavi, T. A.; Tang, Y.; Lin, C.-C.; Manipatruni, S.; Young, I. A.; Datta, S.; Wang, J.-P.; Ramesh, R. Tunable Charge to Spin Conversion in Strontium Iridate Thin Films. *Phys. Rev. Mater.* **2019**, *3*, No. 051201.
(37) Chen, Y.-T.; Takahashi, S.; Nakayama, H.; Althammer, M.; Goennenwein, S. T. B.; Saitoh, E.; Bauer, G. E. W. Theory of Spin Hall Magnetoresistance. *Phys. Rev. B* **2013**, *87*, No. 144411.
(38) Nakayama, H.; Althammer, M.; Chen, Y. T.; Uchida, K.; Kajiwara, Y.; Kikuchi, D.; Ohtani, T.; Geprags, S.; Opel, M.; Takahashi, S.; Gross, R.; Bauer, G. E.; Goennenwein, S. T.; Saitoh, E. Spin Hall Magnetoresistance Induced by a Nonequilibrium Proximity Effect. *Phys. Rev. Lett.* **2013**, *110*, No. 206601.
(39) Althammer, M.; Meyer, S.; Nakayama, H.; Schreier, M.; Altmannshofer, S.; Weiler, M.; Huebl, H.; Geprägs, S.; Opel, M.; Gross, R.; Meier, D.; Klewe, C.; Kuschel, T.; Schmalhorst, J.-M.; Reiss, G.; Shen, L.; Gupta, A.; Chen, Y.-T.; Bauer, G. E. W.; Saitoh, E.; Goennenwein, S. T. B. Quantitative Study of the Spin Hall Magnetoresistance in Ferromagnetic Insulator/Normal Metal Hybrids. *Phys. Rev. B* **2013**, *87*, No. 224401.
(40) Skoropata, E.; Nichols, J.; Ok, J. M.; Chopdekar, R. V.; Choi, E. S.; Rastogi, A.; Shon, C.; Gao, X.; Yoon, S.; Farmer, T.; Desautels, R. D.; Choi, Y.; Haskel, D.; Freeland, J. W.; Okamoto, S.; Brahlek, M.; Lee, H. N. Interfacial Tuning of Chiral Magnetic Interactions. *Sci. Adv.* **2020**, *6*, No. aaz3902.
(41) Yoo, M. W.; Tornos, J.; Sander, A.; Lin, L. F.; Mohanta, N.; Peralta, A.; Sanchez-Manzano, D.; Gallego, F.; Haskel, D.; Freeland, J. W.; Keavney, D. J.; Choi, Y.; Strempfer, J.; Wang, X.; Cabero, M.; Vasili, H. B.; Valvidares, M.; Sanchez-Santolino, G.; Gonzalez-Calbet, J. M.; Rivera, A.; Leon, C.; Rosenkranz, S.; Bibes, M.; Barthelemy, A.; Anane, A.; Dagotto, E.; Okamoto, S.; Te Velthuis, S. G. E.; Santamaria, J.; Villegas, J. E. Large Intrinsic Anomalous Hall Effect in $SrIrO_3$ Induced by Magnetic Proximity Effect. *Nat. Commun.* **2021**, *12*, No. 3283.
(42) Yi, D.; Liu, J.; Hsu, S. L.; Zhang, L.; Choi, Y.; Kim, J. W.; Chen, Z.; Clarkson, J. D.; Serrao, C. R.; Arenholz, E.; Ryan, P. J.; Xu, H.; Birgeneau, R. J.; Ramesh, R. Atomic-scale Control of Magnetic Anisotropy via Novel Spin-orbit Coupling Effect in $La_{2/3}Sr_{1/3}MnO_3/SrIrO_3$ Superlattices. *Proc. Natl. Acad. Sci. U.S.A.* **2016**, *113*, 6397.
(43) Ronetti, F.; Plekhanov, K.; Loss, D.; Klinovaja, J. Magnetically Confined Bound States in Rashba Systems. *Phys. Rev. Res.* **2020**, *2*, No. 022052.
(44) Bhowal, S.; Satpathy, S. Electronic Structure and Anomalous Hall Effect in the Ferromagnetic 3d−5d Superlattice $SrMnO_3/SrIrO_3$. *Phys. Rev. B* **2019**, *99*, No. 245145.
(45) Suraj, T. S.; Omar, G. J.; Jani, H.; Juvaid, M. M.; Hooda, S.; Chaudhuri, A.; Rusydi, A.; Sethupathi, K.; Venkatesan, T.; Ariando, A.; Rao, M. S. R. Tunable and Enhanced Rashba Spin-orbit Coupling in Iridate-manganite Heterostructures. *Phys. Rev. B* **2020**, *102*, No. 125145.
(46) Ovsyannikov, G. A.; Shaikhulov, T. A.; Stankevich, K. L.; Khaydukov, Y.; Andreev, N. V. Magnetism at an Iridate/Manganite Interface: Influence of Strong Spin-orbit Interaction. *Phys. Rev. B* **2020**, *102*, No. 144401.
(47) Meyer, S.; Schlitz, R.; Geprägs, S.; Opel, M.; Huebl, H.; Gross, R.; Goennenwein, S. T. B. Anomalous Hall Effect in YIG|Pt Bilayers. *Appl. Phys. Lett.* **2015**, *106*, No. 132402.
(48) Amamou, W.; Pinchuk, I. V.; Trout, A. H.; Williams, R. E. A.; Antolin, N.; Goad, A.; O'Hara, D. J.; Ahmed, A. S.; Windl, W.; McComb, D. W.; Kawakami, R. K. Magnetic Proximity Effect in Pt/$CoFe_2O_4$ Bilayers. *Phys. Rev. Mater.* **2018**, *2*, No. 011401.
(49) Kresse, G.; Furthmüller, J. Efficiency of Ab-initio Total Energy Calculations for Metals and Semiconductors Using a Plane-wave Basis Set. *Comput. Mater. Sci.* **1996**, *6*, 15−50.
(50) Kresse, G.; Hafner, J. Ab-initio Molecular Dynamics for Liquid Metals. *Phys. Rev. B: Condens. Matter Mater. Phys.* **1993**, *47*, 558−561.
(51) Perdew, J. P.; Burke, K.; Matthias, E. Generalized Gradient Approximation Made Simple. *Phys. Rev. Lett.* **1996**, *77*, 3865−3868.
(52) Anisimov, V. I.; Aryasetiawan, F.; Lichtenstein, A. I. First-principles Calculations of the Electronic Structure and Spectra of Strongly Correlated Systems: the LDA+U Method. *J. Phys.: Condens. Matter* **1997**, *9*, 767−808.
(53) Anisimov, V. I.; Zaanen, J.; Andersen, O. K. Band Theory and Mott Insulators: Hubbard U Instead of Stoner I. *Phys. Rev. B: Condens. Matter Mater. Phys.* **1991**, *44*, 943−954.
(54) Perdew, J. P.; Burke, K.; Yue, W. Generalized Gradient Approximation for the Exchange-correlation Hole of a Many-electron System. *Phys. Rev. B* **1996**, *54*, 16533−16539.
(55) Elsässer, C.; Fahnle, M.; Chan, C. T.; Ho, K. M. Density-functional Energies and Forces with Gaussian-broadened Fractional Occupations. *Phys. Rev. B: Condens. Matter Mater. Phys.* **1994**, *49*, 13975−13978.

https://doi.org/10.1021/acsami.2c01849
ACS Appl. Mater. Interfaces 2022, 14, 15407−15414